Tellus (1982), *34*, 376–384

Calculations of carrier gas effects in non-dispersive infrared analyzers I. Theory

By DAVID W. T. GRIFFITH,[1] *National Center for Atmospheric Research, P.O. Box 3000, Boulder, Colo. 80307, U.S.A.*

(Manuscript received September 21; in final form December 23, 1981)

ABSTRACT

A theory and method of calculation is presented for determining changes in instrument response and hence apparent gas concentration which arise in non-dispersive infrared gas analyzers when gas mixtures with varying carrier gases are analyzed. The theory is based on variations in pressure-broadening in the sample cell of the analyzer and initial comparisons with experimental values for CO_2-in-air and CO_2-in-N_2 indicate good agreement between theory and experiment.

1. Introduction

Non-dispersive infrared (NDIR) gas analyzers have been used for over 30 years in the measurement of atmospheric carbon dioxide concentrations. The collected data have shown significant variations in atmospheric CO_2 concentration, the most significant being a steady increase of ~1 p.p.m. yr^{-1} and an annual cycle of 1 to 15 p.p.m. yr^{-1} depending on latitude. The measurements require a precision of 0.1% or better, which demands extreme care in the operation and calibration of the NDIR analyzers and in the generation and maintenance of concentration standards. The most widely used CO_2 standards are those of the Scripps Institution of Oceanography. These standards are of CO_2 in nitrogen, and it has been recognized for several years that the calibration of NDIR analyzers with these mixtures and subsequent measurement of CO_2 in air leads to systematic relative errors of ~1% (Bischof, 1975; Pearman and Garratt, 1975; Keeling et al., 1976; Pearman, 1977). Since their recognition, these errors have been determined empirically and subsequently used to correct measured CO_2-in-air concentrations for this so-called "carrier gas effect". The effect is known to vary from analyzer to analyzer and with CO_2 concentration and pressure of sample gas, and may vary with other factors such as temperature. For the precise measurements required in atmospheric baseline studies of CO_2, the effect should clearly be well understood to avoid the possibility of hidden systematic errors.

The principles, design, and response of NDIR analyzers have been treated in some detail in a book by Hill and Powell (1968). These authors examined the carrier gas effect in analyzers used for medical measurements of CO_2 at concentrations of a few percent (Chapter 3), but their simplified treatment made assumptions which are incompatible with the precision required for atmospheric baseline CO_2 work. In this paper, a theoretical scheme based on pressure-broadening variations with changes in CO_2 carrier gas is described for the calculation of carrier gas effects using as few physical and numerical approximations as feasible. Whilst the model is applicable to a wide range of uses of NDIR analyzers, comparison with observations is here confined to those of atmospheric baseline CO_2 studies. In the following paper, calculations are compared with experimental results from three different types of analyzer

[1] Present address: Max Planck Institut für Chemie, Postfach 3060, D-6500 Mainz, F.R. Germany.

0040-2826/82/040376-09$02.50/0

(APC[2], URAS[3], UNOR[4]) operated by Keeling and co-workers at the Scripps Institution of Oceanography, U.S.A., and Pearman and co-workers at the CSIRO Division of Atmospheric Physics, Australia. The calculations are sufficiently well in agreement with experiment that some results may be used to suggest more accurate methods of correcting for carrier gas effects in past and future CO_2 data sets.

2. Theory

Fig. 1a shows a schematic view of the sample half of an APC analyzer, the reference half being identical. Infrared radiation from the source is chopped and passed through the sample (or reference) chamber and into the condenser-microphone detector. The diaphragm responds to pressure changes caused by absorption of the chopped infrared beam in the detector, and thus vibrates at the chopping frequency. The movement is detected as a capacitance change between the conducting diaphragm and a fixed electrode. The detector chamber is filled with a CO_2-in-argon gas mixture and is thus sensitized to respond strongly to variations in sample absorption by CO_2 but not by other gases unless their absorption bands overlap those of CO_2 significantly. Infrared beams are passed in-phase down sample and reference paths, and the relative detector outputs are compared by null-balancing electronics to yield the analyzer output. The reference path serves to minimize the possibility of drifts due to changes in ambient conditions.

URAS-type instruments (Fig. 1b) are of similar design, but the detector volumes for sample and reference beams are connected to opposite sides of the same diaphragm. Chopped infrared beams are passed in-phase down both paths, and the diaphragm motion is determined by the balance between sample and reference pressure pulses. The component of detector signal at the chopping frequency is the detector output.

[2] Applied Physics Corporation, Pasadena, California, U.S.A. No longer manufactured, but APC analyzers have been used at Scripps since 1957.

[3] Hartmann & Braun, AG, Postfach 900507, 6 Frankfurt 90, F.R. Germany.

[4] H. Maihak, Semperstrasse 38, 2000 Hamburg 60, F.R. Germany.

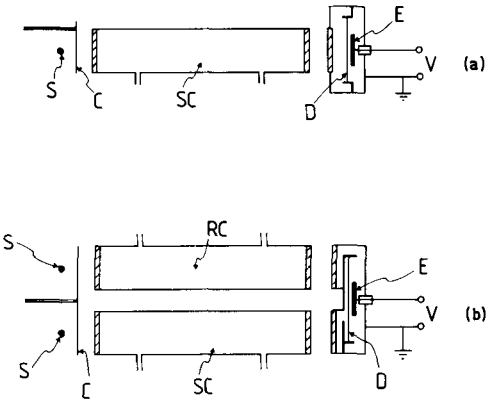

Fig. 1. Schematic diagrams of (a) APC and (b) URAS NDIR analyzers. S = source, C = light chopper, SC = sample cell, RC = reference cell, D = diaphragm, E = fixed electrode, V = output signal.

Hill and Powell (1968, Chapter 2) have treated the response of NDIR microphone detectors theoretically and obtained expressions for the acoustic pressure pulse amplitude developed due to absorption of energy by the filling gas. For conditions pertaining to NDIR analyzer microphones, the pressure pulse amplitude is proportional to the energy absorbed per unit time and volume of detector, and thus depends directly on the total optical absorption in the detector. They have further shown that the microphone output voltage is proportional to the net radiative energy absorbed by the detector. All other parameters affecting detector output are effectively constant in studies of carrier gas effects, so the calculation concentrates solely on changes in energy absorbed in the detector.

The energy absorbed in the detector of an APC or URAS analyzer may be determined by application of the Beer–Lambert Law to the system and integration over the relevant frequency range. Thus the intensity of light of frequency ν emerging from the sample cell, $I_s(\nu)$ (or reference cell, $I_r(\nu)$) is given by

$$I_s(\nu) = I_0(\nu) \cdot \exp[-\kappa_s(\nu) \cdot c_s \cdot l_s] = I_0(\nu) \cdot \exp[-\tau_s(\nu)] \quad (1)$$

where $I_0(\nu)$ is the incident intensity

$\kappa_s(\nu)$ is the absorption coefficient of CO_2 at frequency ν

c_s is the concentration of CO_2 in the sample cell

l_s is the length of the sample cell

and $\tau_s(\nu) = \kappa_s(\nu) \cdot c_s \cdot l_s$ is the dimensionless quantity called optical depth.

For APC and URAS-type analyzers, the intensity absorbed by the detector at frequency ν, $I_a(\nu)$, is

$$I_a(\nu) = I_s(\nu) - I_d(\nu) \tag{2}$$

where $I_d(\nu)$ is the intensity leaving the detector, and $I_s(\nu)$ is assumed to be the intensity incident on the detector. Thus, by applying the Beer–Lambert law again,

$$\begin{aligned} I_a(\nu) &= I_s(\nu) - I_s(\nu) \cdot \exp[-\tau_d(\nu)] \\ &= I_0(\nu) \cdot \exp[-\tau_s(\nu)](1 - \exp[-\tau_d(\nu)]). \end{aligned} \tag{3}$$

The total absorbed energy per unit time in the detector is the integral of (3) over the frequency interval $\Delta\nu$ to which the analyzer responds,

$$A_4 = \int_{\Delta\nu} I_0(\nu) \exp[-\tau_s(\nu)](1 - \exp[-\tau_d(\nu)])\, d\nu. \tag{4}$$

Calculated APC and URAS detector responses are proportional to the difference between A_4 and an analogous integral for the reference path, which is assumed to be constant.

The optical depths $\tau_s(\nu)$ and $\tau_d(\nu)$ in (4) must now be determined from the CO_2 spectrum, which consists of a large number of closely spaced lines in the regions of interest. Each line, i, is described by its centre frequency, ν_{0i}, its temperature dependent strength S_i, and shape function $k_i(\nu)$. CO_2 line shapes near atmospheric pressure are determined by collision broadening and have a Lorentzian shape

$$k_i(\nu) = \frac{\alpha_i/\pi}{(\nu - \nu_{0i})^2 + \alpha_i^2} \tag{5}$$

where α_i is the half-width at half-height. For the ith line the optical depth $\tau_i(\nu) = S_i \cdot k_i(\nu) \cdot c \cdot l$ where c and l are CO_2 concentration and path length, and the total optical depth at any frequency is the sum of contributions from all lines

$$\tau(\nu) = \sum_i S_i \cdot k_i(\nu) \cdot a \tag{6}$$

where $a = c \cdot l$ is the amount of absorber in the path. The optical depths in the sample and detector chambers vary with k_i (through the halfwidth α_i), c and l, and substitution of appropriate optical depths (6) in (4) yields the full form of the integral which must be evaluated.

The integral (4) clearly cannot be evaluated analytically, and numerical methods must be used. In examining carrier gas effects in which CO_2 in carrier gas X is substituted for CO_2 in carrier gas Y at the same concentration in the sample cell, the only input parameter which varies is the CO_2 sample cell line width α_{si}. This line width is determined by collisions and different collision partners have different line-broadening effectiveness. All other inputs to the calculation (except the CO_2 sample concentration) do not, in practice, normally vary from one measurement to another, so we expect that the variation of A_4 with sample cell line widths will explain the carrier gas effects within the limits of the assumptions made in this approach.

Hill and Powell (1968, p. 115 et seq.) treated carrier gas effects by assuming that the detector was so filled that detector response was simply proportional to integrated sample cell absorption. They calculated changes in total sample cell absorption using the data of Burch et al. (1962) for the effect of different broadening gases on total absorption and hence deduced carrier gas effects. However, the true detector response is more precisely determined by (4) and only approximated by the sample cell absorption, and their method is not sufficiently accurate for the precision required in this study.

3. Calculations

Integrals such as (4) cannot be evaluated analytically and there have been many approximate methods (band models) proposed in the past (Goody, 1964; Chapter 4) to estimate integrated absorption in radiative transfer in the atmosphere. Hill and Powell (1968) describe the application of some of these models in predicting NDIR response under various conditions. However, it has proved feasible in this study to evaluate the integrals (4) to excellent numerical accuracy without the use of band model approximations, by evaluating the integrand point by point over the relevant frequency ranges and integrating by Simpson's Rule using a digital computer.

The calculation requires as input the CO_2 spectrum as defined by the line parameters position (ν_{0i}), strength (S_i) and width (α_i), the dependence of the widths on the broadening gas,

the operational temperature T and pressure P, the analyzer sample and detector cell optical pathlengths, and the detector gas mixture composition.

CO_2 absorption line parameters are well known and have been tabulated on magnetic tape by the Air Force Geophysics Laboratory (AFGL) (McLatchey et al., 1973; Rothman, 1978). The line widths on the AFGL tape are derived from a calculation of line widths versus J (rotational quantum number) (Yamamoto et al., 1969) for CO_2-in-N_2. There have also been direct measurements of line widths by several investigators in pure CO_2, N_2, and Ar by tunable laser methods (Arie et al., 1972; Boulet et al., 1972; Boulet et al., 1974; Planet and Tettemer, 1979; Planet et al., 1978; Eng and Mantz, 1979). The measurements for CO_2-in-N_2 are scattered but on average ~12% greater than the values on the AFGL listing. Accordingly, the J-dependence of line widths is assumed here to be that of Yamamoto et al. (1969) but with all values uniformly increased by a factor of 1.12 for CO_2-in-N_2.

For a carrier gas X, we define the carrier gas line-broadening coefficient

$$F(X) = \alpha(X)/\alpha(N_2)$$

where $\alpha(X)$ and $\alpha(N_2)$ are the widths of a line in carrier gases X and N_2 respectively. Band averaged line-broadening coefficients for O_2 and Ar, and the self-broadening coefficient for CO_2, have been determined by Burch, Singleton and Williams (1962) and Burch et al. (1969) relative to N_2 with a stated accuracy of 6%. Values for individual Ar lines are also available from laser measurements (Boulet et al., 1973) and agree fairly well with the average values of Burch et al. (1962). These values are summarized in Table 1. In the calculations of this and the next article a change in carrier gas is simulated by uniformly scaling all J-dependent line widths by a constant carrier gas broadening coefficient. In view of the accuracy to which the line widths are known, I regard this as a reasonable approach. Unfortunately the uncertainties in the carrier broadening factors contribute most of the errors in calculating carrier gas effects.

The analyzer parameters are taken from manufacturers' specifications. Detector fillings for the analyzers studied are approximately known and contain in all cases between 1 and 10% CO_2 in Ar,

Table 1. *CO_2 line-broadening coefficients relative to N_2*

Broadening gas	Integrated absorption measurements	Laser diode measurements
CO_2	1.30,[1] 1.20,[2] 1.30[2]	1.35[3,4]
N_2	(1.00)	(1.00)
O_2	0.81[1]	—
Ar	0.78[1]	0.76[3,5]

The numbers quoted for laser diode measurements are the averages of the appropriate ratios of many individually measured line widths of pure CO_2, CO_2-in-N_2, and CO_2-in-Ar. Refs. 1. Burch et al. (1962). 2. Burch et al. (1969). 3. Boulet et al. (1972). 4. Arie et al. (1971). 5. Boulet et al. (1974).

and it is assumed here that original fillings were to one atmosphere pressure at 296 K.

In evaluating the integral (4) there are three sources of possible numerical error, which have been reduced to insignificant magnitude.

(1) Point spacing in the integrand evaluation. As this parameter is decreased to zero the integral will be calculated exactly but will require infinite time. An interval of 0.02 cm^{-1} (~ one-fifth of a line width) was sufficiently small that a further decrease resulted in less than 1 part in 10^6 difference in the calculated integrals.

(2) Contributions to optical depth at each point. At each evaluated point all CO_2 lines, no matter how distant their centers, contribute to the optical depth. Inclusion of all lines in the summation at all points would make the calculation too time consuming and only lines with centers within a specified distance of the evaluation point are included. With this distance set at 10 cm^{-1} (>100 line widths), errors thus incurred by the neglect of extreme wings of lines are <0.5% in the calculated integral and significant (≤0.01 p.p.m.) in calculated carrier gas effects. Even with a 10 cm^{-1} cut-off, up to 150 lines contribute to the optical depth at some points.

(3) Inclusion of very weak CO_2 lines. Fig. 2 shows the gas phase spectrum of CO_2 at low resolution, in which the major absorption regions near 660, 2350, and 3650 cm^{-1} can be clearly seen. CO_2 lines on the AFGL tape span an intensity range from 3×10^{-18} to

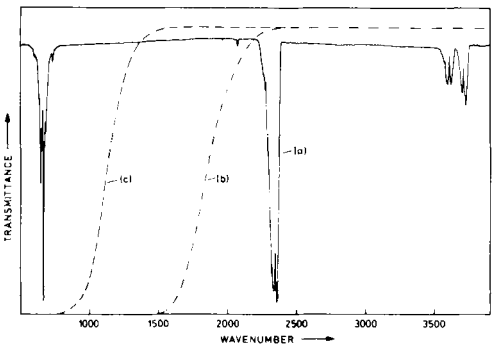

Fig. 2. Low resolution transmittance spectra of (a) CO_2 gas, (b) sapphire, and (c) CaF_2 in the mid-infrared.

2×10^{-26} cm^{-1} (molec cm^{-2})$^{-1}$. The intensity cut-off below which lines were not included in the calculation was normally taken to be 1×10^{-21} cm^{-1} (molec cm^{-2})$^{-1}$ and this set then included 763 lines between 2200–2400 cm^{-1} (ν_3 band) and 3550–3750 cm^{-1} ($\nu_1 + \nu_3$, $2\nu_2 + \nu_3$ bands). Fig. 2 also shows the transmission characteristics of calcium fluoride and sapphire windows used in these analyzers. It can be seen that these materials completely absorb radiation in the 660 cm^{-1} region, and this band can thus be excluded from the calculation. Lowering the cut-off to 10^{-22} cm^{-1} (molec cm^{-2})$^{-1}$ doubled the number of lines but increased calculated absorption only 1%, resulting in an insignificant difference to calculated carrier gas effects.

Finally, it is assumed that $I_0(\nu)$, the source intensity, is constant over the two bands involved and may be removed from the integral. For a black body source at 1000 K the Planck function varies only 4% over the 200 cm^{-1} width of each band, but is about half the value at 3650 cm^{-1} that it is at 2350 cm^{-1}. At 1500 K it is approximately the same in both regions. The constant intensity assumption is made since the temperatures and emission spectra of the sources are unknown. Likely errors arising from this assumption are discussed later.

4. Discussion

The following paper contains a detailed comparison of model calculations and experimental studies of carrier gas effects. In this section a sample calculation is presented for illustrative purposes, the sensitivity of the results to input parameters studied, and a simplified scheme described by which carrier gas effects may be qualitatively predicted.

The sample calculation uses analyzer parameters pertaining to a URAS-2 analyzer (Serial No. 6933216) used by the CSIRO Division of Atmospheric Physics, Australia. This analyzer has a sample cuvette length of 25.0 cm and nominal detector filling of 10% CO_2-in-argon. The detector optical path length is not accurately known; the detector chambers are approximately 1 cm deep and have reflecting polished brass rear walls. Allowing for reflection from the rear wall, the detector optical path length is taken to be 2.0 cm. The analyzer is thermostatted to 60 °C and the sample cell is at atmospheric pressure. The detector is sealed. The line-broadening factors $F(X)$ for $X = O_2$, Ar and CO_2 are taken here from Table 1 as 0.81, 0.78, and 1.3, respectively, relative to N_2. Thus the detector cell line widths, α_{di}, are multiplied by

$$F(\text{det}) = 0.10F(CO_2) + 0.90F(\text{Ar}) = 0.8320$$

and the sample cell line widths, α_{si}, by

$$F(\text{air}) = 0.781 + 0.210 \cdot F(O_2) + 0.009 \cdot F(\text{Ar}) = 0.9581.$$

In laboratory practice the analyzer is calibrated with a suite of standard CO_2-in-N_2 mixtures whose CO_2 concentrations have been determined at the Scripps Institution of Oceanography by comparison with manometrically-determined primary CO_2-in-N_2 standards. Subsequent measurement of a CO_2-in-air sample with the analyzer yields an apparent CO_2 concentration which differs from the true concentration and has been in practice described by a carrier gas shift at a given CO_2 concentration

Δ = apparent CO_2 concentration − true CO_2 concentration.

or by a correction factor

G = true CO_2 concentration/apparent CO_2 concentration.

Carrier gas effects are determined experimentally by comparing analyzer values with true (manometrically determined) CO_2 concentration. In the

following paper we discuss the relative merits of using additive (Δ) or multiplicative (G) corrections, after detailed calculations of carrier gas effects have been described.

The calculation described here follows an analogous procedure: calibration points of A_4 versus α_s (see eqs. (4) and (6)) are firstly calculated in the concentration range of interest with a line-width factor for N_2 ($F(N_2) = 1.00$). Then A_4 is re-evaluated for a given true CO_2 concentration and air line-width factor, the apparent CO_2 concentration is determined from the calibration, and Δ or G determined from the assumed true and calculated apparent concentrations.

Table 2 summarizes calculated carrier gas shifts for 330 p.p.m. CO_2-in-air relative to CO_2-in-N_2 with nominal or best-estimate parameters

Table 2. *Variation of calculated carrier gas shifts with maximum probable changes in input parameters for a URAS-2 analyzer*

Parameter	Standard value	Assumed value for comparison	Carrier gas shift Δ/p.p.m.
All standard (i.e. nominal or best-estimate) values			−4.09
Observed for URAS-2 S/No. 6933216			−4.0 ± 0.4
Detector path length (cm)	2.0	2.6	−4.15
Detector CO_2 mole fraction	0.105	0.100	−4.10
Sample cell path length (cm)	25.0	25.1	−4.10
Argon line-width factor	0.78	0.83	−4.11
Oxygen line-width factor	0.81	0.86	−3.13
Pressure (atm.)	1.00	1.05	−4.06
Temperature (K)	333	336	−4.08
All line strengths +10%			−4.38
All line widths +10%			−3.80
Relative source intensity at 3650 cm^{-1}	1.0	0.5	−4.16
Relative source intensity at 3650 cm^{-1}	1.0	0.0	−4.24

described above, and with each input separately increased to its maximum probable value, to give an idea of expected accuracy of the calculation. Shifts are also calculated assuming that the source intensity at 3650 cm^{-1} is half that at 2350 cm^{-1}, or zero, and the experimentally determined shift is also included for comparison (D. Beardsmore, private communication). It can be seen firstly that the calculated shift agrees well with experiment, and secondly that only the line widths, line strengths and sample line-width factors cause significant (>0.1 p.p.m.) uncertainties, the line-width factors being by far the greatest.

The large uncertainty in the detector path length does not have a large effect because the detector chamber is optically thick and absorption in the detector is nearly saturated, so moderate changes in path length cause only small absorption changes. The neglect of source intensity variation over the two CO_2 bands can also be seen to be minor. Thus the calculation suggests that the effects of a changing source spectrum due, for example, to ageing, voltage fluctuation etc., should be small. Except for the sample line-width uncertainty, Table 2 suggests that the calculation should be able to reproduce observed carrier gas effects within experimental error. The problem of improving the accuracy of the line-width factors is taken up in the following paper where more data are presented.

It is instructive to examine two special cases of (4) which can be solved analytically viz.—those of a spectrum containing only a single line which is either very weak or very strong. For a single very weak line, $\tau(\nu_0) = Sa/\pi\alpha \ll 1$, $\tau(\nu)$ is always $\ll 1$ and $\exp[-\tau(\nu)] \sim 1 - \tau(\nu)$. Then (choosing $\nu_0 = 0$ for convenience, s = sample, d = detector):

$$A_4^{\text{weak}} = \int_{-\infty}^{\infty} \left\{ \frac{Sa_d\,\alpha_d/\pi}{\nu^2 + \alpha_d^2} - \frac{S^2 a_d\,\alpha_d\,a_s\,\alpha_s/\pi^2}{(\nu^2 + \alpha_d^2)(\nu^2 + \alpha_s^2)} \right\} d\nu$$

$$A_4^{\text{weak}} = Sa_d - \frac{S^2 a_d\,a_s}{\pi(\alpha_d + \alpha_s)}. \qquad (7)$$

For a very strong line, $\tau(\nu_0) = Sa/\pi\alpha \gg 1$ and we can approximate (Goody, 1964, Chap. 4)

$$A_4^{\text{strong}} = \int_{-\infty}^{\infty} \exp\left[-\frac{Sa_s\,\alpha_s}{\pi\nu^2}\right] \cdot \left(1 - \exp\left[-\frac{Sa_d\,\alpha_d}{\pi\nu^2}\right]\right) d\nu$$

$$A_4^{\text{strong}} = \sqrt{4S(a_s\,\alpha_s + a_d\,\alpha_d)} - \sqrt{4Sa_s\,\alpha_s}. \qquad (8)$$

As expected, both expressions show decreasing detector absorption as the amount of absorbing gas in the sample cell, a_s, is increased. When $a_s = 0$, $A_4^{weak} = Sa_d$ and $A_4^{strong} = \sqrt{4Sa_s\alpha_s}$ which are respectively the equivalent widths (i.e. integrated absorptions) of lines in the weak- and strong-line limits (Goody, 1964, Chap. 4). The important difference to note is the α_s dependence in eqs. (7) and (8), which is opposite in direction in weak and strong cases. For strong lines an increase in width α_s and an increase in amount a_s have identical effects on detector response, so the broadening of a strong line by a change of carrier gas will result in an apparent increase in CO_2 concentration. For a weak line, however, an increase in α_s will have the same effect as a decrease in a_s, although the variation of A_4^{weak} with α_s is weaker. For URAS and APC analyzers with the cut-off in CO_2 line strengths used in the calculation, the parameters are such that the strongest and weakest lines satisfy the strong and weak limits given above, so in a simple view the observed carrier gas effect will be a balance of opposing effects from weak and strong lines. This view can be very useful in qualitatively estimating the influence of changes in analyzer conditions (temperature, detector filling etc.) on carrier gas effects. Any change which increases the values of $Sa/\pi\alpha$ in the analyzer will tend to move lines from the weak toward the strong limit. Since for strong lines apparent concentrations in air will be lower than those in nitrogen (lines in air are narrower), such a change will decrease apparent CO_2-in-air concentrations relative to CO_2-in-N_2, and increase the magnitude of the carrier gas effect in a URAS-type analyzer. The reverse happens for changes causing a decrease in $Sa/\pi\alpha$.

This principle can be seen to operate in Table 2. Increasing line strengths or any of the path lengths or concentrations increases $Sa/\pi\alpha$, and in all cases the carrier gas effect increases, whilst increasing line widths decreases $Sa/\pi\alpha$ and the carrier gas effect. The lines around 3650 cm^{-1} are medium to weak lines and thus tend to increase apparent CO_2-in-air concentrations relative to CO_2-in-N_2; thus when their contribution is reduced the carrier gas error increases. It should be noted that $Sa/\pi\alpha$ is independent of pressure, so this principle cannot make predictions for pressure changes. With respect to temperature, the amount, a, varies as $1/T$ at constant pressure in the sample cell and is constant in the detector, whilst α varies approximately as $\sqrt{T}$. Thus $Sa/\pi\alpha$ decreases with increasing T, and so does the carrier gas error, even if only slightly.

5. UNOR analyzers

In UNOR analyzers (Luft, 1956; Luft et al., 1967) the detector is also a condenser microphone but there are two detector chambers in series to the infrared beam and connected to opposite sides of a common diaphragm as illustrated in Fig. 3. Absorption in the two detector chambers is carefully balanced; the front chamber is optically much thinner than the rear, and is very sensitive to changes in sample absorption only near the centers of the CO_2 absorption lines whilst the rear chamber is optically thick and relatively insensitive to sample absorption changes. Alternate beams from sample and reference paths are incident on the same detector and the resulting signal modulated at the chopper frequency is the detector output.

Consideration of the absorption in front and rear detector chambers yields respectively

$$I_{af}(\nu) = I_0(\nu) \cdot \exp[-\tau_s(\nu)](1 - \exp[-\tau_f(\nu)]) \quad (9)$$

$$I_{ar}(\nu) = I_0(\nu) \cdot \exp[-\tau_s(\nu)] \cdot \exp[-\tau_f(\nu)] \times (1 - \exp[-\tau_r(\nu)]) \quad (10)$$

with s = sample, f = front detector chamber, r = rear detector chamber. These absorbed intensities give rise to pressure pulses in inverse proportion to their different chamber volumes, V_f and V_r, so the diaphragm motion and detector response will depend on $I_{ar}/V_r - I_{af}/V_f$. The volume factor does not arise in single chamber detectors. The

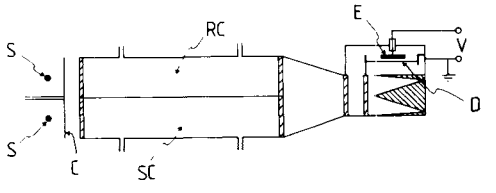

Fig. 3. Schematic diagram of a UNOR NDIR analyzer. S = source, C = light chopper, SC = sample cell, RC = reference cell, D = diaphragm, E = fixed electrode, W = window, V = output signal.

integrated absorption proportional to UNOR response thus becomes (omitting $I_0(\nu)$)

$$A_{11} = \int_{\Delta\nu} \exp[-\tau_s(\nu)] \left(\left(1 + \frac{V_f}{V_r} \right) \cdot \exp[-\tau_r(\nu)] - \frac{V_f}{V_r} \cdot \exp[-\tau_f(\nu) - \tau_r(\nu)] - 1 \right) d\nu \quad (11)$$

and evaluation proceeds by the same method as for (4).

Sample calculations for 330 p.p.m. CO_2-in-air for a UNOR analyzer are summarized in Table 3. The actual analyzer they describe is a UNOR-2, serial No. 631693, also at CSIRO Division of Atmospheric Physics. This analyzer has a 20.0 cm sample cell, a front detector path length of 0.80 cm and a rear detector depth of 3.0 cm. The rear chamber tapers slightly and contains an inverted conical insert, so that radiation undergoes about eight reflections and the total path length is 6.0 cm. The detector is nominally filled with 2.1% CO_2-in-argon. The UNOR instruments are not thermostatted. The active volumes for front and rear chambers are 2.5 cm^3 and 6.5 cm^3 respectively, but the connecting volumes to the diaphragm are uncertain and estimated by the manufacturers to be each 2–3 cm^3. The ratio V_f/V_r is thus estimated to lie in the range 0.45–0.65. The effective optical thicknesses of the two detector chambers are uncertain due to reflective losses in the rear chamber and additional absorption in the front chamber of radiation which has traversed the rear cell. Best estimates of effective front and rear detector optical thicknesses are taken as 0.9 and 5.0 cm assuming 98% reflectivity of the detector walls. The input parameters in Table 3 are varied by estimates of their maximum probable error.

Table 3. *Variation of calculated carrier gas shifts with maximum probable changes in input parameters for a long-cell UNOR-2 analyzer*

Parameter	Standard value	Assumed value for comparison	Carrier gas shift Δ/p.p.m.
All standard (i.e. nominal or best-estimate) values			3.53
Observed for UNOR-2 S/No. 631693			2.7 ± 0.5
Detector volume ratio	0.55	0.65	4.92
Detector CO_2 mole fraction	0.21	0.22	3.24
Front detector path length (cm)	0.9	0.8	4.68
Rear detector path length (cm)	5.0	6.0	3.99
Sample cell path length (cm)	20.0	20.1	3.52
Argon line-width factor	0.78	0.83	3.27
Oxygen line-width factor	0.81	0.86	2.72
Pressure (atm.)	1.00	1.05	3.96
Temperature (K)	296	304	3.22
All line strengths +10%			2.73
All line widths +10%			4.00
Relative source intensity at 3650 cm^{-1}	1.0	0.5	3.54
Relative source intensity at 3650 cm^{-1}	1.0	0.0	3.55

As Table 3 shows, in contrast to the URAS case, the predicted carrier gas errors are much more sensitive to the input uncertainties, although agreement with the measured error is still reasonable with the nominal and best-estimate parameters. The sensitivity to detector geometry is evidently due to the fine balance between absorption in the line centers in the front of the detector and in the wings in the rear chamber. Absolute uncertainty of calculated carrier gas effects for UNOR's will thus be much greater than those for single chamber detector analyzers, but the calculations may still be used to verify and predict many aspects of the behavior of UNOR analyzers.

6. Acknowledgements

The author wishes to sincerely thank G. I. Pearman of CSIRO for much useful discussion, support and co-operation in this work, and C. D. Keeling, R. B. Bacastow and P. R. Guenther of the Scripps Institution of Oceanography for more helpful discussion and co-operation. The author is also indebted to the CSIRO for the award of a CSIRO Postdoctoral Fellowship and to NCAR for a visiting fellowship. The National Center for Atmospheric Research is sponsored by the National Science Foundation.

REFERENCES

Arie, E., Lacome, N. and Rossetti, C. 1971. Spectroscopie par Source Laser I. Etude Expérimentale des Intensités et Largeurs des Raies de la Transition $00°1–(10°0, 02°0)_I$ de CO_2. *Can. J. Phys. 50*, 1800–1804.

Bischof, W. 1975. The influence of the carrier gas on the infrared gas analysis of atmospheric CO_2. *Tellus 27*, 59–61.

Boulet, C., Arie, E., Bovanich, J. P. and Lacome, N. 1972. Spectroscopie par Source Laser II. Etude Expérimentale de l'Elargissement des Raies de la Transition $00°1–(10°0, 02°0)_I$ de CO_2 Perturbé par N_2. *Can. J. Phys. 50*, 2178–2185.

Boulet, C., Isnard, P. and Arie, E. 1974. Largeurs des Raies de la Transition $00°1–(10°0, 02°0)_I$ de CO_2 perturbé par l'Argon. *J. Quant. Spectry. Rad. Transfer 14*, 637–649.

Burch, D. E., Singleton, E. B. and Williams, D. 1962. Absorption line broadening in the infrared. *Appl. Optics 1*, 359–363.

Burch, D. E., Gryvnak, D. A., Patty, R. R. and Bartky, C. E. 1969. Absorption of Infrared Radiant Energy by CO_2 and H_2O. *J. Opt. Soc. Am. 59*, 267–280.

Eng. R. S. and Mantz, A. W. 1979. Tunable diode laser spectroscopy of CO_2 in the 10- to 15-μm spectral region. *J. Molec. Spectry 74*, 331–344.

Goody, R. M. 1964. *Atmospheric radiation.* Oxford: Clarendon Press.

Hill, D. W. and Powell, T. 1968. *Non dispersive infrared gas analysis.* New York: Plenum.

Keeling, C. D., Bacastow, R. B., Bainbridge, A. E., Ekdahl, C. A., Guenther, P. R. and Waterman, L. S. 1976. Atmospheric carbon dioxide variations at Mauna Loa Observatory, Hawaii. *Tellus 28*, 538–551.

Luft, K. F. 1956. Analyse de gaz par absorption infrarouge non dispersive. *Acad. des Sci. Paris., Compt. Rend. 242*, 482–484.

Luft, K. F., Kesseler, G. and Zörner, K. H. 1967. Nichtdispersive ultrarotgasanalyse mit dem UNOR. *Chemie-Ing-Techn. 39*, 937–945.

McClatchey, R. A., Benedict, W. S., Clough, S. A., Burch, D. E., Calfee, R. F., Fox, K., Rothman, L. S. and Garing, J. S. 1973. AFCRL atmospheric absorption line parameters compilation, AFCRL-TR-0096.

Pearman, G. I. 1977. Further studies of the comparability of baseline atmospheric carbon dioxide measurements. *Tellus 29*, 171–181.

Pearman, G. I. and Garratt, J. R. 1975. Errors in atmospheric CO_2 concentration measurements arising from the use of reference gas mixtures different in composition to the sample air. *Tellus 27*, 62–66.

Planet, W. G. and Tettemer, G. L. 1979. Temperature-dependent intensities and widths of N_2-broadened CO_2 lines at 15 μm from tunable laser measurements. *J. Quant. Spectry. Rad. Transfer 22*, 345–354.

Planet, W. G., Tettemer, G. L. and Knoll, J. S. 1978. Temperature dependence of intensities and widths of N_2-broadened lines in the 15 μm CO_2 band from tunable diode laser measurements. *J. Quant. Spectry. Rad. Transfer 20*, 547–556.

Rothman, L. S. 1978. Update of the AFGL atmospheric absorption line parameters compilation. *Appl. Optics 17*, 3517–3518.

Yamamoto, G., Tanaka, M. and Aoki, T. 1969. Estimation of rotational line widths of carbon dioxide bands. *J. Quant. Spectry. Rad. Transfer 9*, 371–382.